Journal of Structural Geology 69 (2014) 108–121

Contents lists available at ScienceDirect

Journal of Structural Geology

journal homepage: www.elsevier.com/locate/jsg

Silica gel in a fault slip surface: Field evidence for palaeo-earthquakes?

Carly Faber [a, *, 1], Christie D. Rowe [a, 2], Jodie A. Miller [b], Åke Fagereng [a, 3], Jan H. Neethling [c]

[a] Department of Geological Sciences, University of Cape Town, Private Bag X3, Rondebosch 7701, South Africa
[b] Department of Earth Sciences, Stellenbosch University, Private Bag X1, Matieland 7601, South Africa
[c] Physics Department, Nelson Mandela Metropolitan University, Port Elizabeth 6001, South Africa

ARTICLE INFO

Article history:
Received 30 May 2014
Received in revised form
9 September 2014
Accepted 14 September 2014
Available online 16 October 2014

Keywords:
Silica gel
Palaeo-earthquakes
Velocity weakening
Fault vein

ABSTRACT

High-velocity friction experiments have shown an almost complete loss of strength associated with silica gel formation on slip surfaces. The identification of frictional silica gel products in palaeo-seismic faults is, however, problematic, because there are multiple natural sources of silica gel and recrystallization of gel to quartz complicates preservation. The importance of gel formation on natural faults is therefore unknown. Here, we report a structurally distinct and semi-continuous, 0.5–10 mm thick layer of microcrystalline quartz along a major carbonate-hosted fault, the Olive fault, in the Naukluft Nappe Complex, Namibia. The quartz layer is distinguished by flow banding-like textures and unusual cathodoluminescence characteristics. The layer consists of ~2–20 μm hexagonal quartz crystals, which include distinct, crystalline, pore-bearing micro-to nano-spheres, separated by pore geometries indicative of volumetric contraction, and with grain boundaries enriched in aluminium. We interpret these features to indicate that the quartz crystals formed from recrystallization and dehydration of a silica gel. Because it is found in a carbonate-hosted fault and crosscuts lithological layering, the silica source is not from comminution of local wall rocks. Rather, the gel likely formed from reshear of a quartz-coated fault surface, or incremental shear slip associated with precipitation of silica driven by co-seismic pressure drops. This example of fault-related silica gel may have formed by a different mechanism than the gels produced in high-velocity friction experiments, but once formed, may have comparable rheological effects.

1. Introduction

Recognizing evidence for past earthquake slip in the rock record is problematic. Other than the presence of pseudotachylyte, which is extremely rare compared to the frequency of earthquakes (Sibson and Toy, 2006; Kirkpatrick et al., 2009; Di Toro et al., 2009; Kirkpatrick and Rowe, 2013), there has been no universally accepted direct field evidence for past seismic slip along faults (Cowan, 1999). Other slip-weakening processes that may record evidence of palaeo-earthquakes have been suggested, such as fluidization of gouge, coseismic carbonate dissociation, and clay breakdown (Otsuki et al., 2003; Rowe et al., 2012; Ujiie and Tanaka, 2013). However, the prevalence of these mechanisms during natural fault slip is not well documented and the evidence can be ambiguous. The formation of hydrous silica gel on slip surfaces has been observed in rock-friction experiments, concurrent with slip-weakening, indicating that silica gel, or its products after diagenesis, may be an alternative indicator of palaeo-earthquakes within the rock record (Goldsby and Tullis, 2002; Di Toro et al., 2004; Hayashi and Tsutsumi, 2010; Di Toro et al., 2011). Recently, a field example of solidified and recrystallized silica gel has been identified in the Corona Heights fault, in San Francisco, California (Kirkpatrick et al., 2013). This study highlighted fault microstructures associated with possible silica gel lubrication, and provides evidence that silica gel may be created in natural fault systems as well as in experiments.

In the experiments, rapid slip weakening was recorded coincident with the formation of the silica gel. The formation of the silica gel was attributed to the presence of moisture, and the slip weakening effect to the thixotropic behaviour of the gel (Goldsby and Tullis, 2002; Di Toro et al., 2004; Hayashi and Tsutsumi, 2010; Niemeijer et al., 2012). However, the few experiments that have been conducted have produced silica gel at a variety of slip rates

* Corresponding author.
E-mail address: carly.faber@uit.no (C. Faber).
[1] Department of Geology, Arctic University of Tromsø, Dramsveien 201, 9037 Tromsø, Norway.
[2] Earth & Planetary Sciences Department, McGill University, 3450 University St., Montreal, QC H3A 0E8, Canada.
[3] School of Earth & Ocean Sciences, Cardiff University, Main Building, Park Place, Cardiff CF10 3AT, United Kingdom.

http://dx.doi.org/10.1016/j.jsg.2014.09.021
0191-8141/

and normal stresses. Goldsby and Tullis (2002) observed it to form at relatively low slip rates (3.2 mm/s), but at high normal stresses (100 MPa), while Di Toro et al. (2004) observed a similar effect at much higher slip rates of 150 mm/s and normal stresses of 5 MPa. Hayashi and Tsutsumi (2010) conducted experiments over a wide range of slip rates (0.87–104 mm/s), and low normal stresses (1.5 MPa), and concluded that slip weakening, concurrent with silica gel formation, only occurred at velocities greater than 40 mm/s. Irrespective of the slip rate, the slip weakening effect caused by the thixotropic behaviour of the gel means that it is a likely mechanism contributing to the increasing slip speeds during an earthquake. However, because silica gel can form at subseismic rates, and because it is only one of a number of weakening mechanisms observed in laboratory experiments, further field and laboratory examples of silica gel in fault zones are required to understand the formation and effects of silica gel during fault slip, and to determine whether this is a prevalent and important process.

In the experiments, the silica gel solidified shortly after shearing ceased, and slip surface observations showed flow textures in the solid silica (Goldsby and Tullis, 2002; Niemeijer et al., 2012). Although the experimental work did not describe other microstructures, studies of cryptocrystalline quartz layers in faults reveal some distinctive features (Ujiie et al., 2007; Kirkpatrick et al., 2013). In addition to flow textures, Kirkpatrick et al. (2013) highlighted fine grain size, presence of nano-scale pores along grain boundaries of larger grains, absence of deformation-induced dislocations, variable degree of crystallinity, and cellular structure within the hydrous crystalline silica as indicating transformation of an amorphous hydrous silica gel to more ordered silica phases. Hydrous silica cements are not uncommon in faults as veins, and distributed within fault breccias, sometimes occurring in large volumes. Many examples have been described in ore deposits or hydrothermal alteration zones associated with volcanic systems (e.g. Power and Tullis, 1989; Caine et al., 2010; Dong et al., 1995; Chi et al., 2006; Sherlock and Lehrman, 1995; Micklethwaite, 2008) and may be formed by fault slip processes or by independent fluid flow. The cements form from silica-rich fluids under conditions where amorphous hydrous silica phases precipitate more rapidly than quartz, even when silica concentrations in hydrothermal fluids are similar to those predicted from quartz solubility models (500–700 ppm; Potapov, 2004). Hydrous silica phases crystallize to opal, chalcedony, and quartz at geologic conditions (Herrington and Wilkinson, 1993), and comparison between natural and laboratory fault materials must take into account the dehydration and crystallization experienced by hydrous silica over geologic time at shallow crustal temperatures.

Since the experimental discoveries, structural geologists have been seeking ways to distinguish frictionally produced silica gels from other amorphous silica found in faults, but further work is necessary. The primary microstructures of fault-slip related silica gel are likely to be somewhat different to silica gels formed by biological or sedimentary processes due to their formation under shear stress. However, the primary microstructures formed during the solidification of the amorphous phase may be preserved during dehydration and crystallization (e.g. Oehler, 1975), and could be used to recognize recrystallized amorphous silica (Ujiie et al., 2007; Kirkpatrick et al., 2013). It must be noted that amorphous material has also been developed in slow (10^{-5}–10^{-4} mm/s) creep experiments, conducted at mid-crustal conditions (Pc ~ 500 MPa, T = 300 °C). In these experiments, deformation localized into anastomosing slip surfaces, on which partially amorphous material was observed. At higher strains, deformation localized further into one or two layers. These layers contained completely amorphous material. Both the partially amorphous and amorphous material were interpreted to form by comminution and amorphization under high pressure (Pec et al., 2012). Given the range of slip rates, and conditions at which it may be produced, the rate dependence of formation of amorphous silica is still uncertain, even if amorphous silica can be shown to have formed frictionally.

This study focusses on a microcrystalline quartz layer in a ~500 Ma fault in the Naukluft Nappe Complex, Namibia (Fig. 1). The quartz layer occurs in carbonate fault rocks and therefore the source of silica is not as straightforward as in the chert-hosted example presented by Kirkpatrick et al. (2013), or in the experimental studies that all deformed quartz rocks (Goldsby and Tullis, 2002; Di Toro et al., 2004; Hayashi and Tsutsumi, 2010). Here, we describe the microstructures of the fault-hosted quartz layer in detail, and present arguments for its formation by frictional generation of silica gel on the fault surface. We then speculate on the mechanism by which silica gel may have formed and discuss three non-exclusive possibilities for its origin: (1) silica gel formed during cataclasis by comminution and hydrolization as in experiments (e.g. Goldsby and Tullis, 2002; Di Toro et al., 2004); (2) silica gel formed by precipitation during gradual fluid advection along the fault (Caine et al., 2010; Power and Tullis, 1989); and (3) silica gel formed by on-fault reactions concurrent with slip (Herrington and Wilkinson, 1993). The shear-weakening rheology documented by the silica gel-forming experiments indicate that regardless of the mode of formation, silica gels on fault surfaces are likely to have significant slip-weakening effects (Goldsby and Tullis., 2002; Di Toro et al., 2004; Kirkpatrick et al., 2013). They are therefore potentially important indicators of dynamic weakening on natural faults.

2. Geological context

The Naukluft Nappe Complex (NNC) in central western Namibia, forms part of the Damara Orogen, a Neoproterozoic to Cambrian orogenic belt associated with collision between the Congo Craton to the north and the Kalahari Craton to the south (Fig. 1a) (Coward, 1981; Gray et al., 2008). Collision resulted in northwest subduction of the Kalahari Craton underneath the Congo Craton at around 530 Ma (Gray et al., 2006), producing an asymmetric bivergent orogenic belt (Coward, 1981). South of the central collision zone are a series of tectonostratigraphic zones (Miller, 1983), associated with development of an accretionary prism above the subduction zone, a fold and thrust belt and a southern foreland basin. The accretionary prism and fold and thrust belt are composed of Damaran sediments, whereas the southern foreland basin, which developed on the Kalahari Craton, was filled with sediments of the lower Phanerozoic Nama Group (Miller, 1983; Gray et al., 2006, 2008). The folded and faulted sediments of the NNC show similarities to both the older Damara sequences and the younger Nama Group (Hartnady, 1978; Martin et al., 1983) and probably represent an early depositional phase in the foreland basin somewhere between 550 and 750 Ma (Miller, 1983).

The NNC (Fig. 1a) is made up of a series of stacked nappes composed of unmetamorphosed to very low grade dolostones, shales, and quartzites with minor volcaniclastics, conglomerates and breccia (Korn and Martin, 1959; Martin and Porada, 1977; Hartnady, 1978; Barnes and Sawyer, 1980; Miller, 1983; Viola et al., 2006). These nappes were emplaced southeastward over the southern foreland basin along the basal Naukluft thrust at around 530 - 480 Ma, and later incised and exhumed to form the thrust klippe of the Naukluft Mountains (Ahrendt et al., 1983; Stanistreet et al., 1991; Gray et al., 2006). Ahrendt et al. (1978) concluded that maximum temperature experienced by the NNC was probably not higher than 350 °C. These estimates are for biotite-bearing rocks in the north of the NNC. The temperature

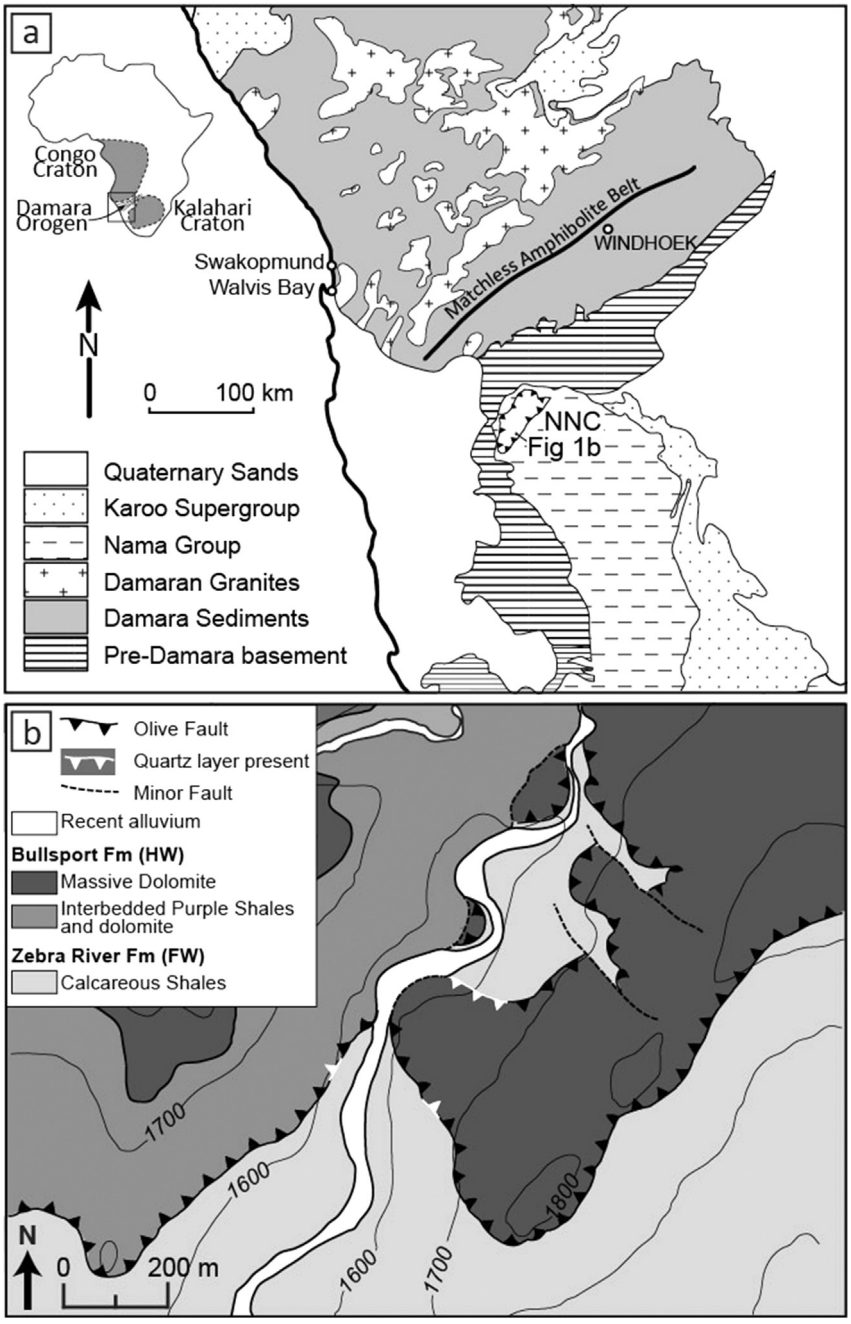

Fig. 1. (a) Regional geological context of the Naukluft Nappe Complex within the geological framework of Namibia; (b) Geological map of the study area showing the mapped length of the Olive fault from this study and the outcrop distribution of the quartz layer along its length.

estimates decrease towards biotite-absent rocks in the SE in the region of our study area. Unfortunately these estimates were conducted using uncalibrated illite crystallinity, and are therefore not quantitative. However, the presence of clay-wrapped quartz aggregates described by Ahrendt et al. (1978), and the lack of biotite in the south-eastern NNC metasediments, suggest that the temperature of burial did not exceed 100–150 °C, and that the rocks reached ca. 2–5 km depth.

3. Analytical and imaging techniques

Microstructural characterization of the quartz layer was performed using a multi-technique approach including x-ray diffraction (XRD), scanning electron microscopy (SEM), transmission electron microscopy (TEM), and cold cathodoluminescence (CL) imaging. XRD was performed on bulk rock powders in the Department of Geological Sciences at the University of Cape Town, using a Philips PW1390 Powder Diffractometer. Spectra were collected with CuKα radiation at 25 V and 40 mA with 1° diffraction slit, 0.02° steps and count times of 0.5 s per step. Spectra were processed and analysed using Panalytical X'Pert software.

Scanning electron microscopy was performed in the Electron Microscopy Unit at the University of Cape Town with the Leica S440 SEM. The instrument operated at 20 keV and 800 pA, using a tungsten filament. All TEM imaging was performed in the Department of Physics at the Nelson Mandela Metropolitan University.

Samples were prepared by conventional grinding and polishing followed by argon milling until electron transparency was achieved. All TEM imaging was performed using a 200 kV Philips CM20 TEM.

4. Fault description

In the SW part of the NNC, a nappe-bounding thrust fault separates hanging wall massive dolostones of the Büllsport Formation from calcareous shales and minor dolostones of the Zebra River Formation (Fig. 1b). The thrust fault damage zone is characterized by mélange fabrics in the footwall shale, and local coarse breccias and high fracture intensity in the hanging wall dolostone. The fault core occurs as a ~20–50 cm thick layer of cohesive dolomitic breccia, which is semi-continuous along the fault, bounded by calcareous shale below. The lower boundary of the dolomitic breccia layer is wavy and the layer varies in thickness along the fault plane. Fault zone Riedel shears, folding, and roughness anisotropy on the hanging wall contact indicate top-to-the-SE displacement. Although the local geometry of the thrust is complicated by offset on later faults, this transport direction is consistent with the regional transport direction in the nappe complex (Korn and Martin, 1959; Hartnady, 1978). Given the slip-parallel extent of the thrust sheet forming the hanging wall, the total fault displacement can be constrained to a minimum of 25 km.

Along one section of this nappe-bounding fault (Fig. 2a), locally and informally named the Olive fault (Rowe et al., 2012), a fine-grained quartz layer with sharp boundaries occurs as a distinct, semi-continuous, sub-planar horizon (Figs. 2b, c). The layer forms a boundary between the hanging wall dolomitic breccia above, and the fault core breccia below. The dolomite breccias above and below the quartz layer differ in their mineralogy, their degree of incorporation of the hanging wall and footwall rocks, and their degree of healing. Occasionally, when the fault core breccia below the quartz layer tapers to zero thickness, the quartz layer crosscuts the shale footwall material and the shear fabrics therein (Fig. 2b). The quartz layer was located in three sections over a 2 km stretch along the Olive Fault (Fig. 1b). Within each of these three sections it is continuous, with the longest unbroken length occurring along 20 m of the fault strike outcrop. It is, however, traceable in sections extending to ~50 m of outcrop length (Fig. 1b). Where it ends, it is most often cut off by other faults. However in one place it is observed to thin and taper to zero thickness. The layer is a distinct solitary horizon with no offshoots or splays (Fig. 2b). It is tabular and variable in thickness between 0.5 and 10 mm, and has sharp boundaries (Figs. 2c, d). For comparison, we searched for similar quartz or silica veins outside the principal slip surface and found only one antitaxial, blocky to fibrous quartz vein, which cuts the hanging wall dolostone two metres above the main fault (Fig. 2e). Other veins around the fault include abundant calcite and dolomite veins within the dolomite hanging wall, and less prevalent calcite veins in the footwall shales. All veins are typically tensile and oriented at high angles to the fault surface, with the majority being less than 1 mm wide.

To better determine the mineralogy of the quartz layer, fault core breccia, hanging wall dolostone breccia, and footwall shale, the mineral content of each was characterized by XRD (Fig. 3). Sample NF13 was taken from the footwall calcareous shales. Hand sample NF08 contained hanging wall dolostone breccia, fault core breccia, and the quartz layer. The sample was trimmed to isolate these three components and powdered for analysis. The hanging wall dolostone breccia is composed almost entirely of dolomite, with minor quartz and albite. The major minerals detected in the footwall rock are quartz, illite, chlorite, albite and calcite, consistent with the field identification of low-greenschist facies calcareous shale. In the fault-core breccia, only dolomite, minor calcite and albite were in detectable quantities (detection limit ~ a few %). However, microcrystalline quartz clasts are observed in the breccia in thin section. CL imaging (Fig. 4) of the different fault components also revealed differences between the breccia below the quartz layer and the hanging wall dolostone breccia above it. The fault core breccia contains more turquoise-luminescing detrital quartz grains and fine-grained violet-luminescing microcrystalline quartz clasts (mostly near the quartz layer), as well as yellow-orange luminescing carbonate (Fig. 4), which is absent in the hanging wall breccia.

5. Microstructural characterisation of the quartz layer

The quartz layer is generally composed of bands of equant quartz crystals of varying, but typically <20 μm, grain size (Fig. 5a). The margins are characterized by wispy bands of distinctly finer grain size (<2 μm), at low angle to or parallel to the edges of the layer (Fig. 5a). The interior of the layer is characterized by slightly larger quartz grains (5–20 μm) with hexagonal to subhedral grain shapes (Figs. 5b, 6a and 6b). Insertion of the tint plate shows no preferred shape or crystallographic orientation. The layer also contains no visible fluid inclusions. Locally, fine-grained dolomite replaces quartz in irregular patches. The hanging wall breccia above the quartz layer contains coarse-grained dolostone fragments and some quartz, cemented by coarse-grained dolomite. The fault core breccia below is finer grained and contains dolostone clasts, shale fragments, and some clasts of microcrystalline quartz, cemented by dolomite and calcite (Figs. 5c, d). The microcrystalline quartz clasts are only found in the fault core breccia near the quartz layer (consistent with CL observations) (Fig. 5c). The quartz layer is also cut by microfaults with <1 mm offset (Fig. 5e). In contrast to the quartz layer, the single quartz vein in the area has crack-seal texture defined by wall-parallel tracks of solid inclusions (mostly dolomite fragments) in elongate blocky quartz crystals that are considerably coarser than the surrounding host rock (Fig. 5f).

5.1. Mineralogy

The mineralogy of the quartz layer was determined by XRD. To do this, the thickest area of the quartz layer was selected and the wall rock trimmed away to within a few millimeters of the quartz layer. This sample was then cleaned of excess carbonate wall rock by bathing it in warm HCl for 24 h. Analysis of the XRD spectra shows that the quartz layer consists almost entirely of quartz, with traces of dolomite, and no detectable amorphous material (Fig. 3). The trace dolomite is attributed to the presence of ~10 μm euhedral dolomite grains completely encased within the quartz layer, and therefore protected from dissolution during sample preparation. CL imaging of the quartz layer revealed subtle variations in its mineralogical characteristics. The different grain-size bands within the layer have distinct CL characteristics (Fig. 4). The main band of hexagonal-shaped to subhedral quartz grains luminesces violet-blue, whereas the finer-grained material found along one or both edges is isotropic in transmitted light and luminesce creamy white in CL. Small dolomite crystals are included in the quartz layer, revealed in the CL image by bright red luminescence (Fig. 4).

5.2. Porosity

The quartz layer is porous, and pores can be described in two different classes. Larger pores in the silica layer are 2–5 μm across, have no clear preferred orientation or elongation, and occur at grain boundary junctions. The majority of the pores are smaller than the quartz grains (Fig. 6). Although we cannot rule out the possibility

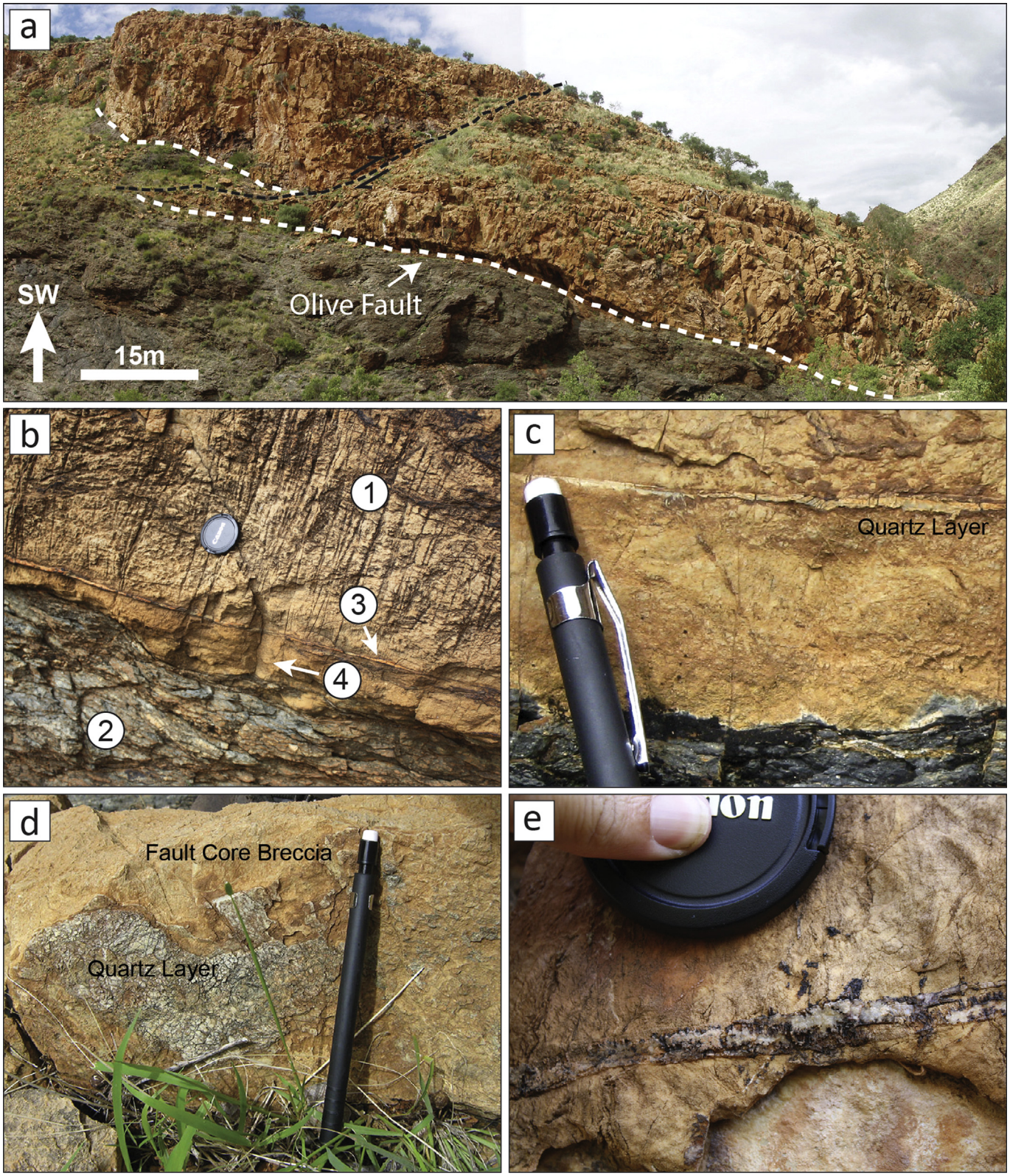

Fig. 2. Field relations of the Olive Fault and the quartz layer. (a) view to the SW of the Olive Fault, indicated by dashed white line, with Büllsport Formation Dolomite in the hanging wall and Zebra River Formation calcareous shales in the footwall. The Olive Fault is offset by a later fault indicated by the black dashed line; (b) fault stratigraphy of the quartz layer in outcrop including hanging wall dolostone healed breccia (1), footwall shale (2), fault core including planar quartz layer (3) and fault core breccia (4); (c) close up of the quartz layer showing subtle variations in thickness within the overall planar layer; (d) outcrop showing the planar quartz layer in plan view, partially eroded away, revealing fault core breccia below; (e) single example of a blocky quartz vein found within the mapped area of the silica fault layer (two metres above the fault surface in dolostone hanging wall).

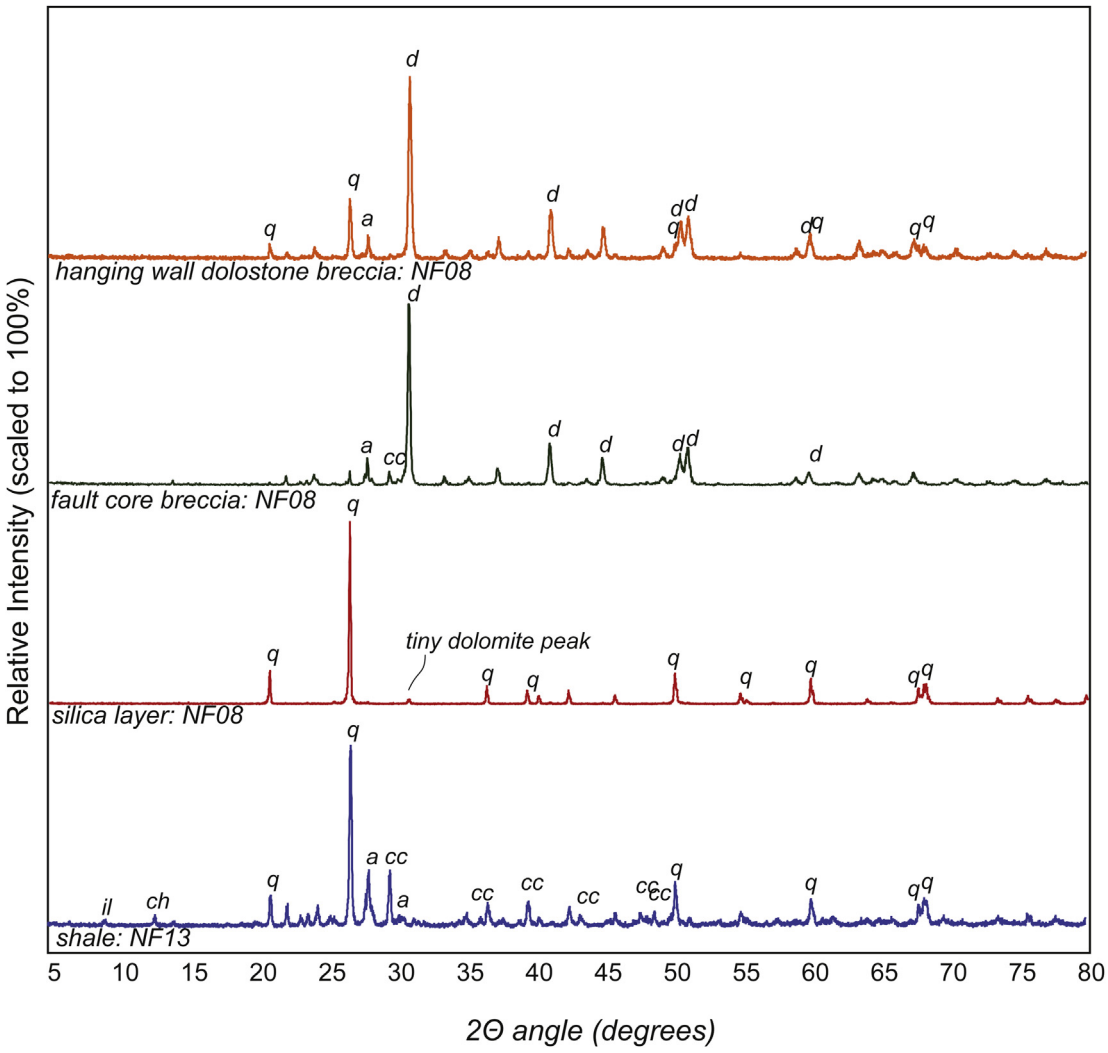

Fig. 3. X-ray diffraction spectra of wall rock and fault rock samples with peaks identified, presented in structural order from hanging wall dolostone healed breccia (top) through fault core (2nd and 3rd spectra) to the footwall (bottom). The hanging wall dolostone healed breccia contains predominantly dolomite (d) with minor quartz (q) and albite (a). The fault core breccia contains dolostone, calcite (cc), and albite, with very small peaks suggesting traces of quartz and an unidentified phyllosilicate. The silica layer contains quartz and trace dolomite. The footwall shale contains quartz, calcite, illite (il), chlorite (ch) and albite, and an unidentified phyllosilicate. Note that due to bulk sample packing, the peaks for phyllosilicates (including illite and chlorite) are not to scale with respect to their relative abundances (as compared to the other minerals).

that some of the large pores were created by plucking of quartz grains during thin section preparation, most appear to be primary. Typically, quartz grains have a more hexagonal shape than the large pores, and with straighter walls, while the large pores have more convex walls or irregular shapes. The large pores are also mostly smaller than the typical quartz crystals. The smaller pores only occur along grain boundaries and are elongate, with a <0.6 μm–long axis parallel to the grain boundary (Fig. 6 and inset). Since we cannot know exactly how many of the large pores formed by grain plucking, we present a maximum estimate for total porosity by pixel counting on SEM images thresholded to bitmaps using Adobe Photoshop and Image-J 1.42q (Fig. 6). After manual image adjustment and thresholding, pores were auto-detected using Gray Scale Image Analysis code for Matlab (Bjørk, 2006a, b). Pores were counted and measured for long and short axes, orientation, and area. Two thin sections across the silica layer, cut perpendicular to one another, were imaged. Four images were analysed (two from each thin section), and the pore area % estimates for each image are as follows: 13.8 area % (1095 pores; image area 194 by 132 μm), 14.5 area % (519 pores; image area 89 by 61 μm), 13.3 area % (706 pores; image area 133 by 91 μm) and 12.4 area % (191 pores; image area 53 by 37 μm) (mean = 13.5 ± 0.9%). The variability in the porosity measurements may reflect spatial heterogeneity on the scale of the SEM images used for counting.

The translation from 2D pore area to 3D pore volume depends on pore size and shape distribution, and the orientation and position of the 2D plane of observation through the 3D volume. Since the cross-section viewed in the 2D image will usually intersect a pore at less than its maximum diameter, 2D pore area estimates typically underestimate 3D pore volume (Sahagian and Proussevitch, 1998). Thus, our analysis likely underestimates the true porosity of the samples, but some fraction of these pores may have been created during sample handling, resulting in an overestimate of true porosity. Neither of these effects are thought to introduce errors more than ~25%.

We emphasize that the important observation is that the quartz layer is porous, and similar in nature to that observed by Kirkpatrick et al. (2013) in the Corona fault silica layer. As we describe here, Kirkpatrick et al. (2013) showed two different types of pores; 1) angular, sub-micrometer sized pores between quartz

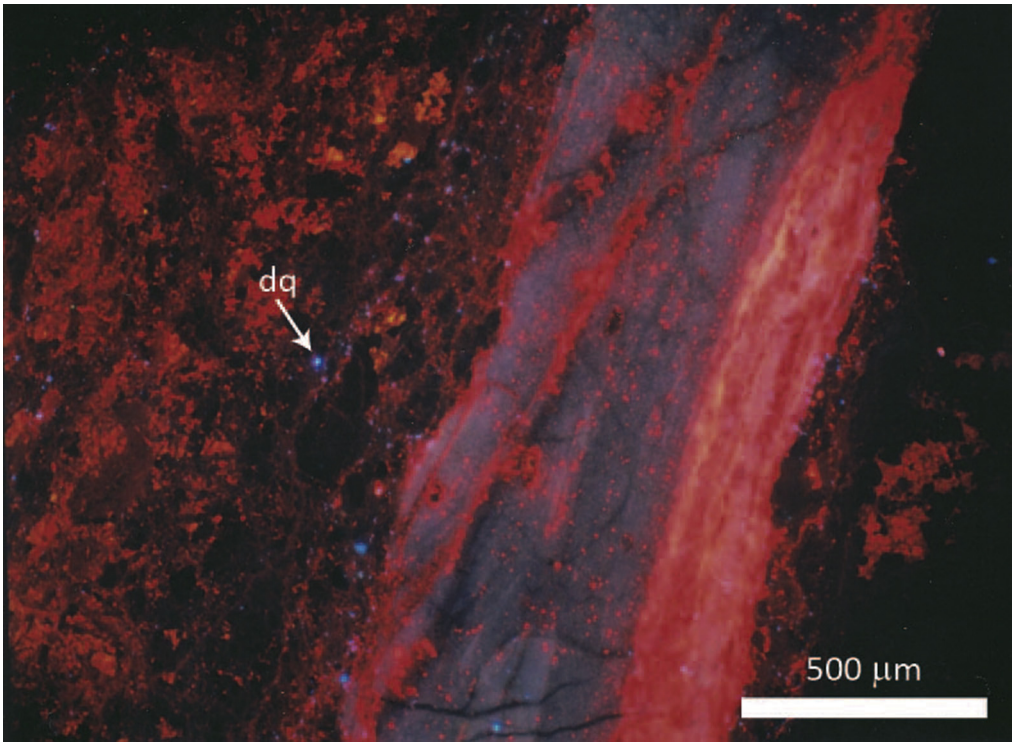

Fig. 4. Cold cathodoluminescence image of silica layer, with fault core breccia to the left, and hanging wall dolostone breccia to the right of the quartz layer. Dolomite luminesces bright red or dark blackish red. Bright blue specks (dq) in wall rock are detrital quartz grains. Quartz layer, and small microcrystalline quartz clasts luminesce violet to white (dolomite crystals included in the quartz layer are bright red). In general, violet-luminescing areas are coarser grained than white-luminescing areas (corresponding to banding in Fig. 3a). (For interpretation of the references to colour in this figure legend, the reader is referred to the web version of this article.)

grains, and 2) elongate nanometer-scale pores along quartz grain boundaries. In addition, our porosity estimates are only 1–2% higher than porosity associated with volumetric contraction during opal-CT dehydration in diagenetic settings, estimated at 12% (Moore and Vrolijk, 1992).

5.3. Nanospheres

The subhedral to hexagonal quartz grains locally have monocrystalline silica inclusions about 100–200 nm in diameter (Fig. 7a). These inclusions are spherical to ellipsoidal, and sometimes exhibit a single pore on their surface (Fig. 7b). Some inclusions have a rim of smaller quartz spheres (~30 nm) (Fig. 7c). The rounded inclusions are single crystals with the same α-quartz electron diffraction pattern as the quartz grains, but energy dispersive spectrometry (EDS) analysis indicates ~7% aluminium and 4–7% potassium are present, as well as oxygen and silicon. The aluminium and potassium are only found within the rounded inclusions, not in the surrounding quartz crystals. The quartz has a very low density of dislocations, but where present, dislocations appear to be concentrated around the inclusions (e.g. Fig. 7a and c). It is worth noting that this is consistent with the study of Kirkpatrick et al. (2013) who also found that quartz, inferred to have recrystallised from hydrous silica gel, had no or very few dislocations within the crystal structure.

6. Origin of the quartz layer

The field setting of the quartz layer, cutting parallel to and within a major regional fault surface, within fault breccias, suggests that it is fault-related. The thin quartz layer separates breccias derived only from hanging wall rocks, from breccias of mixed hanging wall and footwall lithologies. This separation is supported by the presence of orange-yellow luminescing carbonate, observed in CL, exclusively within the fault core breccia below the quartz layer. In carbonates, material that luminesces yellow, interstitial to red luminescent dolomites, usually represents later crystallization of a carbonate (Adams and Mackenzie, 1998). The presence of recycled microcrystalline quartz clasts in the fault core breccia (Fig. 3c) provides evidence for cataclastic recycling of previous fault-related quartz layers, and the sharp, planar, nature of the quartz layer indicates that it formed in the final slip event within the fault core, likely with a maximum displacement estimate of no more than a few metres. Given the criteria described above, we interpret that the quartz layer occupies the final principal slip surface, similar to those documented in studies of other major faults (e.g. the Punchbowl Fault, Chester and Chester, 1998).

The microcrystalline texture, wispy banding, porosity, presence of nanospheres and low dislocation density within the quartz layer are characteristics rarely observed in typical hydrothermal quartz veins (c.f. Bons et al., 2012). The assemblage of microstructural characteristics is therefore better explained by evolution from a silica gel, which solidified as a hydrous silica layer (probably opal), and later recrystallized to anhydrous quartz. In the inferred evolution from a silica gel to the observed quartz layer, the wispy banding is interpreted as a flow texture formed during fault slip (c.f. Stel and Lankreyer, 1994). The continuous patterns of banding across the quartz layer indicate that if this is indeed flow banding, the complete thickness of the layer comprises one generation of silica gel. The cold cathodoluminescence colour of the quartz layer (Fig. 5) is unusual for quartz, with colours ranging from violet to white more typically reported in high temperature igneous or metamorphic quartz grains that have cooled quickly (Götze et al.,

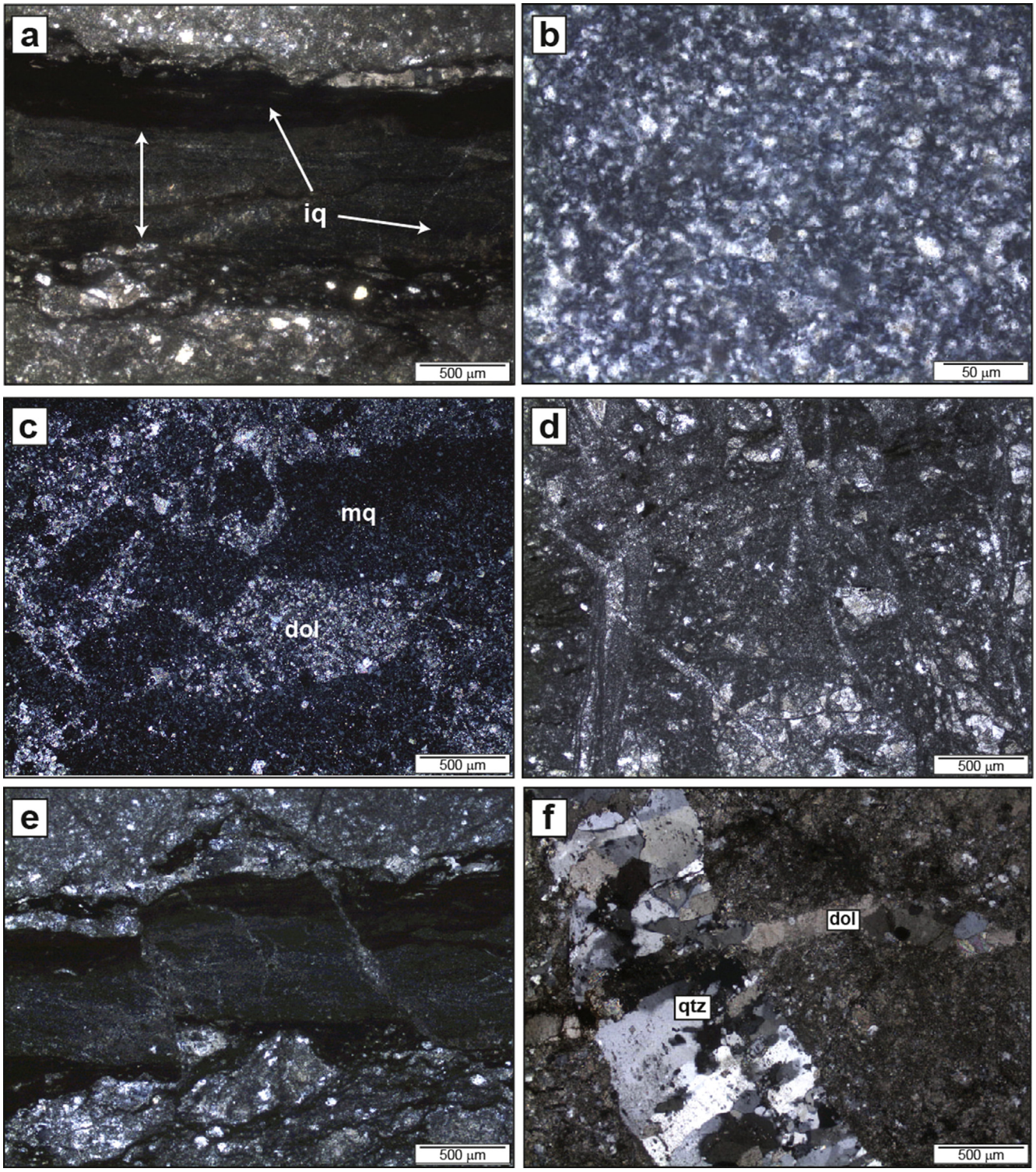

Fig. 5. Photomicrographs of the quartz layer. (a) XPL image of the quartz layer, with white, double-sided arrow indicating the width of the layer. The dark material along the upper edge and within the layer (iq) is quartz that appears isotropic in a standard 30 μm thin section due to very fine grain size. Note grain size banding through centre of quartz layer (inclined bands of coarser quartz crystals visible at centre and left in lower half of quartz layer); (b) A close-up XPL image of the microcrystalline quartz grains that comprise the central part of the quartz layer; (c) XPL image of angular clasts of microcrystalline quartz (mq) amongst the dolostone clasts (dol) in the fault core breccia near the margins of the quartz layer; (d) PPL image of clasts and fragments of dolomite within the fault core breccia; (e) XPL image of microfaults offsetting the quartz layer; and (f) XPL image of blocky crack-seal texture in quartz vein (qtz) found in hanging wall dolostone, cross cut by late dolomite vein (dol). Note the difference in primary microtexture between the crack-seal vein (f) and the quartz layer in (a, b, e).

2001). The fine grain size and possible flow textures are distinct from the only blocky-fibrous quartz vein found outside the fault zone (Fig. 2f), and from veins associated with the basal Naukluft thrust (Fagereng et al., 2014), and within our knowledge of the NNC, unique to this single fault surface. Blocks of microcrystalline quartz similar to the fault layer are also observed as angular clasts in the fault core dolostone breccia (Fig. 3c), demonstrating possible recycling of previous quartz layers in the fault.

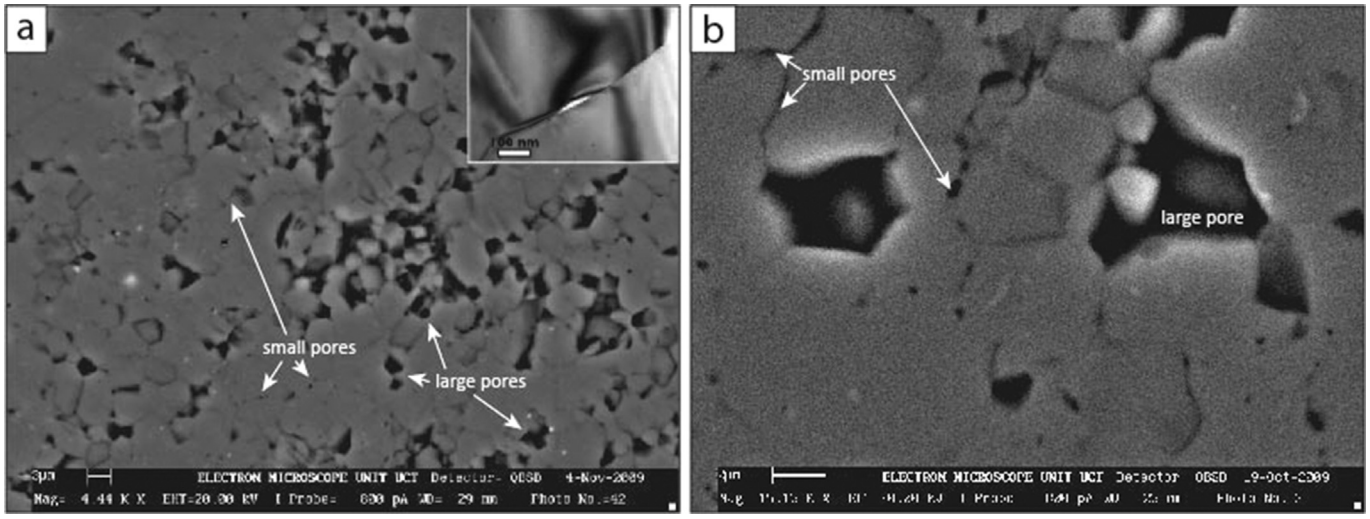

Fig. 6. SEM images and TEM image (inset) of pore structures within the silica layer. (a) Main image is an SEM photo of porosity structure in silica layer. Equant hexagonal grains are delineated by strings of <1 μm scale pores along boundaries and 5–20 μm pores at grain boundary intersections. Inset: TEM image of small grain boundary pore. (b) Close up on pore structure displaying delineation of grain boundaries by planar arrays of micropores.

In silica-saturated solutions, opal precipitation is particularly favoured at low temperatures and high rates of precipitation or solidification (White et al., 1956), and through the presence of carbonates that inhibit quartz precipitation by reducing the pH (White and Crerar, 1985; Colby et al., 1986). Silica solutions can nucleate opaline spherules without needing foreign particles for growth (Jorge et al., 2005). When a fluid is supersaturated with such particles, solid amorphous silica is formed exhibiting micron- to submicron-scale spheroidal texture (Oehler, 1976).

Opal and other amorphous silica species can include substantial Al concentrations, far in excess of the impurities normally found in α-quartz (Oehler, 1976; Mroczek et al., 2000). During hydrothermal crystallization experiments of opaline silica to microcrystalline quartz, Oehler (1976) observed the presence and conservation of 1–10 μm spheres. These microspheres contain 72–83% quartz with other silica phases, and in some cases exhibit a pore-like hole on the surface that may have allowed water escape during recrystallization. In the quartz layer, some of these microspheres are preserved, despite recrystallization to single crystals of quartz. The high concentrations of Al and K preserved in the microspheres are evidence for impurities inherited from a primary opaline phase.

The microspheres are isolated inclusions within the 5–20 μm hexagonal to subhedral quartz crystals. These tiny individual crystals are invisible in transmitted light and appear similar to chert. Natural partially crystalline silica has been reported to have a honeycomb or foam microstructure (Herrington and Wilkinson, 1993). This microstructure has been shown experimentally to convert to anhedral quartz grains comprising “artificial chert” at temperatures of ~100–300 °C and pressures of 3 kbar (Oehler, 1976), conditions compatible with the burial conditions of the Olive fault wall rocks (Ahrendt et al., 1978). Oehler (1976) also points out that in natural chert, grain boundaries of newly formed

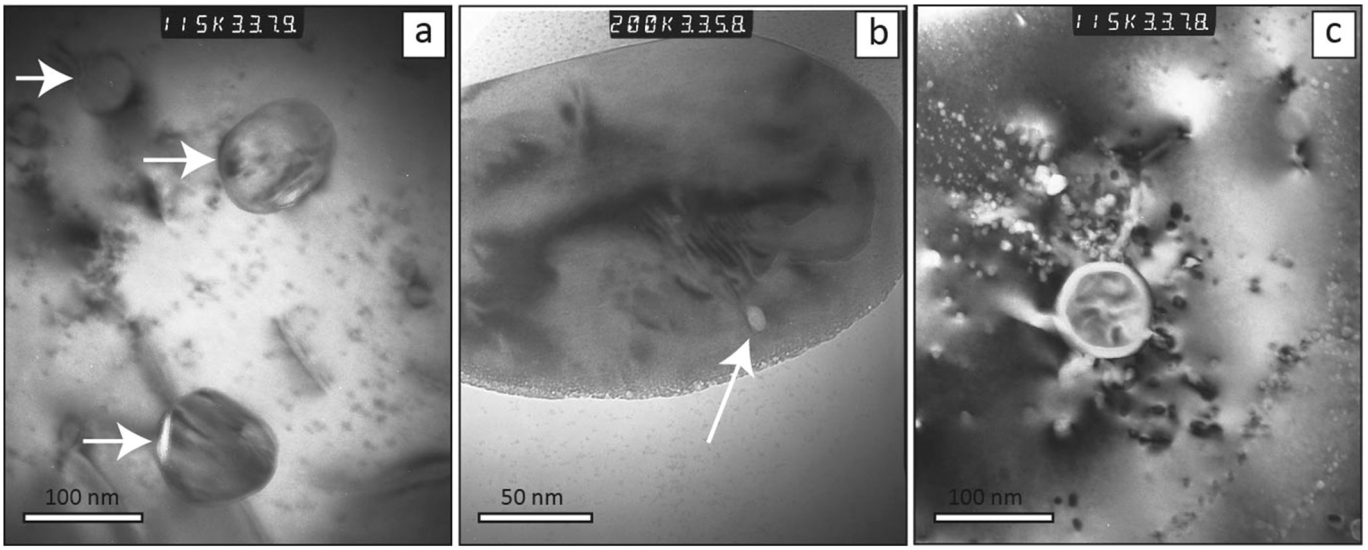

Fig. 7. TEM images of nanospheres within quartz grains in the silica fault layer. (a) Several single-crystal nanospheres (arrows) within a quartz crystal that shows a low density of dislocation loops; (b) Close-up of a nanosphere inclusion. The bright ellipse at lower right is a pore, or hole, in the ultrathin TEM sample and probably represents a pore in the nanosphere; (c) A nanosphere inclusion with a bright crystalline rim.

anhedral quartz grains are independent of primary microspheres and may either include microspheres or grow across the microsphere boundaries.

The density of dislocations in the quartz crystals in the layer is extraordinarily low, and the dislocations occur, at least in places, as dislocation loops (Figs. 7a and c) that indicate minor post-crystallization deformation of the quartz grains. We suggest that these nearly strain-free quartz grains formed during dehydration and static recrystallization of a primary opaline layer. The porosity in the quartz layer (13.5 ± 0.9%), even when taking into account the uncertainties introduced by sample plucking and extrapolation from 2D images, is on the same order as the volumetric contraction associated with opal-CT dehydration of quartz in diagenetic settings (~12%; Moore and Vrolijk, 1992). In this interpretation, the pores found at triple junctions and along grain boundaries formed by contraction of the silica as individual crystals transformed to quartz, and water escaped from the quartz layer.

Microcrystalline fault veins and cements have been reported in several other locations. Ujiie et al. (2007) described a single, few tens of μm to 100 μm-thick, microcrystalline (1–10 μm grain-size) silica layer in a fault comprising basaltic rocks in the Shimanto accretionary complex, southwest Japan. Similar to the quartz layer described here, the layer is planar, contains fine-grained isotropic (cryptocrystalline) quartz, is absent of grain-shape fabrics, and grains have a low dislocation density and spherical nanometer-sized single-crystal quartz inclusions. Ujiie et al. (2007) attributed the genesis of the layer to crystallization from a silica gel that formed by supersaturation of fluids infiltrated into the fault zone.

In the Stillwater Fault, Dixie Valley, Nevada, Power & Tullis, (1989) and Caine et al. (2010) may also describe a silica gel vein that has undergone subsequent deformation on a fault slip surface (Power and Tullis, 1989). The silica gel was interpreted as deposited by hydrothermal fluids along a leaky normal fault, and the resultant vein was modified by solution creep, yielding a crystallographic preferred orientation. Similar to the Olive fault quartz layer, the Stillwater Fault vein is composed of 0.01–1 μm quartz crystals with very low dislocation densities. However, in contrast to Power and Tullis (1989), we observed no crystallographic preferred orientation in the quartz layer.

Kirkpatrick et al. (2013) showed equant, submicron quartz and amorphous silica in a thin flow-banded layer in the Corona Fault, San Francisco. The quartz crystals also contained spheroidal silica particles, similar to those we describe in the Olive fault. Kirkpatrick et al. (2013) also interpreted these as evidence for a gel-phase precursor to the microcrystalline quartz. The wall rock to the Corona fault is chert, so the silica gel may form by a similar mechanism as the weakening observed in chert grinding experiments (e.g. Goldsby and Tullis, 2002). All of our observations indicate primary gel microtextures that are unaffected by subsequent solution creep or crystal plastic deformation, and which result from, and were modified by, static recrystallization and dehydration. Caine et al. (2010) also showed that the microcrystalline quartz occurred as a component of the cement in cemented fault breccias of the Stillwater fault, whereas in the Olive fault, the fault in the Shimanto accretionary complex, and the Corona fault, microcrystalline quartz is only found on the principal slip surface. The comparison between these four faults, however, raises the question of how a silica gel can form along a principal slip surface in quartz-poor wall rock.

7. Formation of the silica gel

Natural hydrous silica gels occur in hot springs, around volcanic vents, in epithermal veins associated with volcanic fluids, and during diagenesis of sediments containing biogenic hydrous silica grains (e.g. Humphris et al., 1995; Poetsch, 2004; Weibel et al., 2010). In the case of magmatic sources, these gels are formed by advection of silica-rich fluids to higher crustal levels, where phase separation may concentrate the dissolved silica as pressure and temperature decrease. As there are no known magmatic rocks or hydrothermal deposits associated with the rock units in the area of this fault, and the inferred silica gel is confined to a single fault slip surface, we consider it highly unlikely that this silica gel had a magmatic origin and do not investigate this possibility further. In sedimentary diagenesis, silica gels are derived from biogenic opal. As the wall rocks to the fault were metamorphosed at low greenschist facies prior to development of the fault, no biogenic silica could have been present in the wall rocks before faulting. Thus, we discard biogenic origins as a possible explanation for the silica layer.

The 0.5–10 mm thick, fine-grained quartz layer reported here, that we interpret as a recrystallized silica gel, is confined to a single fault plane that cross-cuts other diagenetic and tectonic structures. This occurrence implies that the formation of the inferred silica gel is related to conditions during slip on this fault surface. Therefore, we explore three possible mechanisms of silica gel formation: (1) local comminution and hydration as observed in friction experiments; (2) advection of high-silica fluids from deeper structural levels up the fault during transient high permeability; and (3) the *in situ* production of a gel by concentration of locally derived silica by reactions along the fault surface.

7.1. Silica gel formed by local comminution and hydration

In experiments performed on quartz-rich rocks silica gel was generated on the slip surface at slip rates of a few to hundreds of mm/s (Goldsby and Tullis, 2002; Di Toro et al., 2004; Hayashi and Tsutsumi, 2010; Niemeijer et al., 2012). Although the exact mechanism of formation is not well understood, it almost certainly involves grain size reduction by cataclasis (Hayashi and Tsutsumi, 2010). Silica gels formed in this way are thixotropic, such that their viscosity decreases with increasing slip rate (Goldsby and Tullis, 2002; Di Toro et al., 2004; Hayashi and Tsutsumi, 2010). This property of experimental fault-related silica gels may be important on natural faults regardless of how the silica gel forms. The wall rocks to the Olive fault are dolostone and calcareous shale, and the immediate edges of the quartz layer are dominantly dolostone breccias. The breccias contain a fraction, <15%, of quartz and other silicate minerals. Thus, it is difficult to see how a relatively small and dispersed volume fraction of silicate minerals in the wall rock could form a concentrated silica layer along the fault by comminution. If the silica source was cataclasis of the immediate wall rock, it is more likely that the fine-grained quartz layer defining the slip surface would also contain other minerals, from comminution of calcareous shale and dolostone. It is therefore unlikely that the inferred silica gel formed by cataclasis and hydration of the wall rock.

7.2. Precipitation due to isothermal fluid advection

Previous studies of amorphous silica deposits have suggested that advection of fluids along faults from higher pressure/temperature conditions can result in supersaturation and precipitation (e.g. Bons, 2001; Caine et al., 2010; Power and Tullis, 1989). We consider the possibilities of silica deposition by advection, and local reactions along the fault plane, by calculating silica solubility in aqueous solution as a function of temperature and pressure following the model of Manning (1994). To calculate the density of water, as a function of temperature and pressure, we used the Compensated-Redlich-Kwong equation of state for H_2O (Holland

and Powell, 1991). This is not an attempt at high resolution calculations of silica solubility in a complex fault system, but an attempt at order-of-magnitude semi-quantitative estimates of the feasibility of silica precipitation from a number of scenarios, assuming silica saturated, aqueous fluids of negligible salinity were present at depth below the location of the inferred silica gel.

If a silica-saturated fluid travels up a fault along some geothermal gradient, the equilibrium silica solubility (K) will decrease as a result of decreasing temperature and pressure (Fig. 8a) (Manning, 1994). If a silica gel layer precipitated at 5 km depth, a silica-saturated fluid must have travelled more than 5 km vertically, i.e. originate at depths in excess of 10 km, to experience an order of magnitude decrease in silica solubility (measured as equilibrium molality). If the silica gel precipitated at 1–2 km depth, the solubility may decrease by several orders of magnitude over a few hundred meters of advective flow. Because the Olive fault locally dips 20°, 1 km vertical transport is equivalent to approximately 3 km of along-fault transport. The required vertical transport distance increases with decreasing geothermal gradient (Fig. 8a).

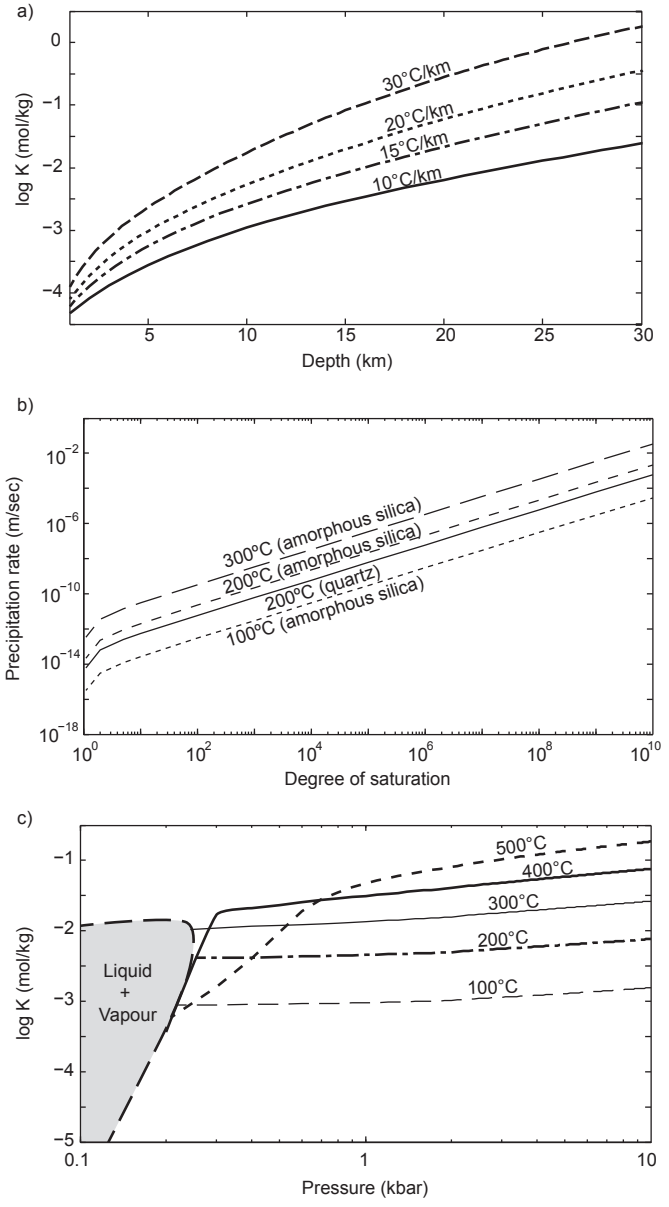

Fig. 8. Plots of quartz solubility and precipitation rates, following empirical relations of Manning (1994) and Rimstidt and Barnes (1980). a) Log of equilibrium constant K, which represents the equilibrium molality of aqueous silica, as a function of depth, plotted along a number of geothermal gradients; b) Precipitation rate expressed as the rate of increase in thickness for a continuous quartz/opal layer (Eq. (1)), as a function of the degree of saturation, S, a defined as dissolved silica in an aqueous fluid, divided by equilibrium solubility; c) Log K as a function of pressure, contoured for temperature. Note the potential for a significant drop in solubility at the liquid + vapour field as pressures decrease toward 100 bar.

In order to assess possible fluid advection rates, we compare observations of fluid venting in active accretionary wedge systems, which have similar low-angle thrust geometry, and derive fluids from pore water in underthrust saturated sediments. Brown et al. (2005) measured the flow from submarine vents on the Costa Rica margin and determined background flow rates of 10^{-6}–10^{-4} cm/day, with prolonged spikes up to 10^{-3} cm/day apparently triggered by slip events on nearby faults. Tryon et al. (2002) measured background rates (not associated with rupture events) at active fault-guided seeps on the order of cm/yr.

At these rates, along-fault transport would require millions of years, or direct vertical flow, several hundred thousands of years, to transport sufficient silica to build the Olive fault silica vein. In addition, slow transport would allow sufficient time for thermal equilibration and nucleation of more ordered species, and would therefore be expected to precipitate quartz veins such as the one in Figs. 2e and 3f continuously along the transport path. If advection happened episodically and flow rates were comparable to precipitation rates (i.e. flow is not the rate-limiting factor), for example in episodic earthquakes leading to transient increases in permeability, we can constrain the rate of precipitation of a quartz vein. The rate of surface growth of a planar quartz layer can be expressed as (Rimstidt and Barnes, 1980):

$$r_{sfc} = kV_{qtz}(1 - S) \quad (1)$$

where k is a temperature-dependent rate constant, V_{qtz} is the molar volume of quartz (22.55 cm^3/mol) and S is the degree of saturation, defined as the activity product of dissolved quartz in the silica-bearing fluid divided by the equilibrium solubility (K). Therefore, if equilibrium solubility is an order of magnitude less than the concentration of dissolved silica in the fluid, and assuming activity of H_2O is one, then S is 10. Fig. 8b shows precipitation rate against temperature for various degrees of saturation, as calculated using Eq. (1). If precipitation occurs at 200 °C ambient temperature, then the equilibrium rate of quartz growth is on the order of tens of μm per year (Fig. 8b). Therefore, even if sufficient fluid volume was not a problem, and the fluid is supersaturated by a factor of 10, it would still take tens to hundreds of years to precipitate a one millimeter-thick quartz layer at equilibrium. Advection is therefore not a viable mechanism for precipitating a layer of quartz under isothermal conditions. However, it is not impossible that a quartz layer did precipitate slowly over hundreds of years, and was later reworked during slip.

The problem of fluid volume and advection rates in forming quartz veins (of much larger volumes) was addressed by Bons (2001) using the formulation of Secor and Pollard (1975) for the migration of water-filled cracks. Bons (2001)'s model estimates migration velocities of ~1 m/s for hydrofractures, implying that negligible precipitation may occur over these short time scales. Although this may be an effective mechanism for bringing high-silica fluids into the upper crust, the process is limited to small volumes of fluid in each batch, and is driven by density gradient. Thus, the shallowly dipping, thin vein in the Olive Fault may not be the ideal scenario for application of the Bons model, but we do not categorically rule out the possibility of rapid advection in a pulse-like hydrofracture.

7.3. Gel formation in situ due to on-fault reactions due to slip

As described above, gel formation is most often caused by supersaturation. It is observed in many geologic environments when solvent (in this case water) is removed from the solution. In hydrothermal vents, this may be driven by evaporation or freezing upon eruption (Channing and Butler, 2007). At depth, a similar effect may occur when a phase separation in the fluid results in the supersaturation of silica in one of the phases, for example when depressurization causes boiling of pore fluids (Sander and Black, 1988). After vapor separation, the remaining aqueous solution may be highly supersaturated, form colloids and deposit hydrous silica. These reactions have been invoked to explain silica alteration and veining in fault-hosted gold deposits; for example, Herrington and Wilkinson (1993) interpreted anhedral quartz grains containing spheroidal inclusions to indicate that fault veins had been precipitated from a silica gel after a rapid pressure drop.

Reports of silica textures in epithermal systems are interpreted to record *in situ* boiling causing formation of colloid-bearing silica sols, which solidify to gels, and are later partially or fully dewatered to quartz (Dong et al., 1995; Potapov, 2004; Ronacher et al., 2000). In addition, the pH of the fluid, affected by wall rock chemistry, may also affect the likelihood of silica gel formation. The wall rocks to the Olive fault are dolomitic, and may be expected to release CO_2 during frictional slip even at subseismic rates (Dickinson et al., 1991), lowering the pH. Low pH inhibits the nucleation of α-quartz, and facilitates precipitation of hydrous silica (Hinman, 1990).

Decreasing pressure also affects equilibrium silica solubility. However, for any constant temperature, changing pressure from as much as 10 kbar–1 kbar has a negligible effect, a factor of two at the most (Fig. 8c). There is, however, a significant effect if pressure drops sufficiently to enter the field of flash vaporization, by entering the liquid + vapour stability field (Fig. 8c). In this case, solubility changes of four to five orders of magnitude are feasible, allowing precipitation rates to move into the realm of micrometers in seconds to minutes (Fig. 8b). In this case, it is possible to rapidly precipitate a quartz layer. However, the solubility in the silica-saturated, local fluid, is only going to be on the order of 10^{-2} mol/kg at 300 °C (Fig. 8b), or less at lower temperatures. Such molalities are not sufficient to precipitate a millimetres thick quartz layer with a reasonable volume of fluid. It is possible to create a quartz layer in this manner, for example by episodic earthquake slip and repeated quartz precipitation over 10s–100s of slip events, but it is not possible in a single event (c.f. Weatherley and Henley, 2013). To reach precipitation rates capable of producing a millimeter-thick quartz or amorphous silica layer in the order of minutes, a degree of saturation, *S*, of 8–10 orders of magnitude is needed (Fig. 8b). However, the solubility before the pressure drop is still only on the order of 10^{-2} mol/kg, such that an unreasonably high volume of silica-saturated fluid (>4500 kg of water per square meter of fault area) is required to obtain a sufficient silica budget. There may be conditions in CO_2-rich, acid environments where high silica saturation is possible. Coupled with a very significant pressure drop associated with flash vaporization, it may then be possible to obtain 8–10 order of magnitude silica supersaturation and a sufficient silica budget (e.g. Herrington and Wilkinson, 1993). It is, however, much simpler to explain the observed silica layer by repeated slip and reworking of a quartz layer that grows incrementally over multiple slip and precipitation events, particularly in our example where the carbonate wall rock provides a very limited silica supply. The observation of quartz fragments in the dolomitic breccia supports this interpretation (Fig. 3c).

7.4. Preferred model for silica gel formation and implications for fault slip

It does not seem possible that the quartz layer, interpreted here to be a fossil silica gel, formed by quartz or opal precipitation in a single event. A thin layer may have formed by boiling, i.e. flash vaporization, related to a rapid co-seismic pressure drop, but not the full observed thickness of the layer (0.5–10 mm). However, if we accept the interpretation that the quartz layer represents a recrystallized silica gel, then there must be a mechanism for its generation. The lack of extensive quartz veining suggests a general shortage of silica in the system; however, because detrital quartz is present in the footwall shales, it is possible that solution mobilization of some quartz contributed material to the silica layer (c.f. Fisher and Brantley, 1992). The simplest explanation seems to be comminution and hydrolization as observed in experiments. If this is true, then a silica layer must have been there before the slip event that created the silica gel. There are two ways of achieving this: (1) the quartz layer represents a quartz vein that precipitated from deeply-derived fluids moving along the fault, and became a gel during a slip event along the now quartz-coated slip surface; or (2) the layer grew episodically by flash vaporization during slip events, and the observed layer reflects slip in the last of these events, where previous slip events are not preserved because the layer gets reworked in each event. Option (1) appears less probable, because this mechanism would likely have led to the formation of more quartz veins in the surrounding rock. Option (2) is more consistent with the observation that the microcrystalline silica is only found on the fault surface, because this relates silica deposition to slip-surface conditions. The presence of reworked clasts of microcrystalline silica near the quartz layer (Fig. 3c) favours option (2), demonstrating that small deposits of microcrystalline silica were brecciated in subsequent slip events. However, in all considered, possible scenarios, there is a requirement that before the last slip event, there was already a quartz layer present along the fault.

8. Conclusions

This study has reported the presence of a microcrystalline quartz layer along a carbonate fault surface. The quartz layer has microstructures consistent with preservation from an initial amorphous phase followed by dehydration (and associated volume loss) during static recrystallization to microcrystalline quartz. The structural occurrence as a thin, planar, semi-continuous fault-zone-parallel layer that cross-cuts all other structures, absence of any similar materials outside the fault core, lack of volcanic or hydrothermal activity in the area, and the isolation of the quartz layer in a predominantly carbonate setting are all consistent with the generation of the quartz layer during fault slip.

Pore structures inferred to record volume loss during dehydration to quartz, and elevated K and Al content in microsphere inclusions, are consistent with an opal species as the primary solid silica phase, and imply that the quartz layer originated as a fault-related silica gel. These features may distinguish quartz veins formed from solidification and dehydration of silica gels from ordinary quartz veins precipitated in equilibrium from aqueous fluids. Cases of other carbonate-hosted faults where opaline cements have been suggested to record silica gel formation (e.g. the Zuccale Fault and Naukluft Thrust; Smith et al., 2011; Rowe et al., 2012) may also be explained by this model.

It is intriguing that the inferred silica gel has formed along a slip surface within dolomitic host rocks, with no obvious silica source. We suggest two options for how the quartz layer originated: (1) it formed by precipitation of quartz along the fault surface by advection, either in multiple episodes, or slowly and continuously

to form a quartz layer that was later reworked to a gel; or (2) it formed by episodic flash vaporization events and associated silica precipitation during a number of slip events. Neither of these mechanisms can explain the thickness of the quartz layer without invoking either a pre-existing quartz layer, or multiple slip events. We therefore conclude that the inferred silica gel formed in the last slip event on the fault, by slip along a pre-existing quartz layer that may or may not have experienced repeated episodes of gel formation to achieve its current thickness.

Acknowledgements

This work is supported by National Science Foundation grant 0840977 to Rowe and Emily Brodsky, NRF Grant 65296 to Miller, and a University of Cape Town Postgraduate Publication Grant to Faber. We thank Fernando Sylvester and Nils Backeberg for help with mapping and discussions in the field, and Charlotte Bate for assistance with image processing. Thanks to Miranda Waldron for help with the scanning electron microscope, Ronel August for XRD scanning, and David Wilson, Rene van der Merwe, and Ernest Stout for sample preparation. We gratefully acknowledge Giulio di Toro, Johann Diener, and Kohtaro Ujiie for helpful discussions, and Heather Savage and James Kirkpatrick for insightful comments on this manuscript. Thanks to Dr Ben Mapani and the staff at Parks Namibia for organizing restricted area permits to work in the Naukluft National Park, and to Kohtaro Ujiie and an anonymous reviewer for helpful insights on this manuscript.

References

Ahrendt, H., Behr, H.-J., Clauer, N., Hunziker, J.C., Porada, H., Weber, K., 1983. The Northern Branch: depositional development and timing of the structural and metamorphic evolution within the framework of the Damara Orogen. In: Martin, H., Eder, F.W. (Eds.), Intracontinental Fold Belts. Springer-Verlag, pp. 723–743.

Ahrendt, H., Hunziker, J.C., Weber, K., 1978. Age and degree of metamorphism and time of nappe emplacement along the southern margin of the Damara Orogen/Namibia (SW-Africa). Geol. Rundsch. 67 (2), 719–742.

Barnes, S.-J., Sawyer, E.W., 1980. An alternative model for the Damara Mobile Belt: Ocean crust subduction and continental convergence. Precambrian Res. 13, 297–336.

Bjørk, T.E., 2006a. Gray Scale Image Analysis. In: Image Analysis Program for Use with MATLAB. http://folk.uio.no/torbjoeb/image_analysis/.

Bjørk, T.E., 2006b. Quantification and Modeling of Deformation Processes: Motivated by Observations from the Contact to the Hornelen Basin, Bremangerland. Masters thesis. Physics of Geological Processes (PGP), Department of Physics, University of Oslo. http://folk.uio.no/torbjoeb/master_thesis.

Bons, P.D., 2001. The formation of large quartz veins by rapid ascent of fluids in mobile hydrofractures. Tectonophysics 336, 1–17.

Bons, P.D., Elburg, M.A., Gomez-Rivas, E., 2012. A review of the formation of tectonic veins and their microstructures. J. Struct. Geol. 43, 33–62.

Brown, K.M., Tryon, M.D., DeShon, H.R., Dorman, L.M., Schwartz, S., 2005. Correlated transient fluid pulsing and seismic tremor in the Costa Rica subduction zone. Earth Planet. Sci. Lett. 238, 189–203.

Caine, J.S., Bruhn, R.L., Forster, C.B., 2010. Internal structure, fault rocks, and inferences Dixie Valley, Nevada. J. Struct. Geol. 32, 1576–1589.

Channing, A., Butler, I.B., 2007. Cryogenic opal-A deposition from Yellowstone hot springs. Earth Planet. Sci. Lett. 257, 121–131.

Chester, F.M., Chester, J.S., 1998. Ultracataclasite structure and friction processes of the Punchbowl fault, San Andreas system, California. Tectonophysics 295, 199–221.

Chi, G., Dubé, B., Williamson, K., Williams-Jones, A.E., 2006. Formation of the Campbell-Red Lake gold deposit by H2O-poor, CO_2-dominated fluids. Miner. Deposita 40, 726–741. http://dx.doi.org/10.1007/s00126-005-0029-3.

Colby, M.W., Osaka, A., Mackenzie, J.D., 1986. Effects of temperature on formation of silica gel. J. Non-Crystal. Solids 82, 37–41.

Cowan, D.S., 1999. Do faults preserve a record of seismic slip? A field geologist's opinion. J. Struct. Geol. 21, 995–1001.

Coward, M.P., 1981. The junction between Pan African mobile belts in Namibia: its structural history. Tectonophysics 76, 59–73.

Di Toro, G., Goldsby, D.L., Tullis, T.E., 2004. Friction falls toward zero in quartz rock as slip velocity approaches seismic rates. Nature 427, 436–439.

Di Toro, G., Pennacchioni, G., Nielsen, S., 2009. Pseudotachylytes and earthquake source mechanics. In: Fukuyama, E. (Ed.), Fault-zone Properties and Earthquake Rupture Dynamics, International Geophysics Series, vol. 94. Elsevier Academic Press, pp. 87–133. ISBN-13: 978-0-12-374452-4.

Di Toro, G., Han, R., Hirose, T., Paola, N.D., Nielsen, S., Mizoguchi, K., Ferri, F., Cocco, M., Shimamoto, T., 2011. Fault lubrication during earthquakes. Nature 471, 494–498. http://dx.doi.org/10.1038/nature09838.

Dickinson, J.T., Jensen, L.C., Langford, S.C., Rosenberg, P.E., Blanchard, D.L., 1991. CO_2 emission accompanying the fracture of calcite. Phys. Chem. Minerals 18, 320–325.

Dong, G., Morrison, G., Jaireth, S., 1995. Quartz textures in epithermal veins, Queensland – classification, origin, and implication. Econ. Geol. 90, 1841–1856.

Fagereng, Å., Smith, Z., Rowe, C.D., Makhubu, B., Sylvester, F.Y.G., 2014. Stress, strain, and fault behavior at a thrust ramp: Insights from the Naukluft thrust, Namibia. J. Struct. Geol. 58, 95–107.

Fisher, D.M., Brantley, S.L., 1992. Models of quartz overgrowth and vein formation: deformation and episodic fluid flow in an ancient subduction zone. J. Geophys. Res. 97 (B13), 20,043–20,061.

Gray, D.R., Foster, D.A., Goscombe, B., Passchier, C.W., Trouw, R.A.J., 2006. $^{40}Ar/^{39}Ar$ thermochronology of the Pan-African Damara Orogen, Namibia, with implications for the tectonothermal and geodynamic evolution. Precambrian Res. 150 (1–2), 49–72.

Gray, D.R., Foster, D.A., Meert, J.G., Goscombe, B.D., Armstrong, R., Trouw, R.A.J., Passchier, C.W., 2008. A Damara orogeny perspective on the assembly of southwestern Gondwana. Geol. Soc. London Spec. Publ. 294, 257–278.

Goldsby, D.L., Tullis, T.E., 2002. Low frictional strength of quartz rocks at subseismic slip rates. Geophys. Res. Lett. 29 (17), 1844–1847.

Götze, J., Plötze, M., Habermann, D., 2001. Origin, spectral characteristics and practical applications of the cathodoluminescence (CL) of quartz – a review. Mineral. Petrol. 71, 225–250.

Hartnady, C.J.H., 1978. The stratigraphy and structure of the Naukluft Nappe Complex. In: Precambrian Research Unit Annual. University of Cape Town Department of Geology, pp. 163–170.

Hayashi, N., Tsutsumi, A., 2010. Deformation textures and mechanical behavior of a hydrated amorphous silica formed along an experimentally produced fault in chert. Geophys. Res. Lett. 37 (L12305) http://dx.doi.org/10.1029//2010GL042943.

Herrington, R.J., Wilkinson, J.J., 1993. Colloidal gold and silica in mesothermal vein systems. Geology 21, 539–542.

Hinman, N.W., 1990. Chemical factors influencing the rates and sequences of silica phase transitions: effects of organic constituents. Geochimica Cosmochimica Acta 54, 1563–1574.

Holland, T., Powell, R., 1991. A Compensated-Redlich-Kwong (CORK) equation for volumes and fugacities of CO_2 and H_2O in the range 1 bar to 50 kbar and 100–1600 °C. Contrib. Mineral. Petrol. 109, 265–273.

Humphris, S.E., Herzig, P.M., Miller, D.J., Alt, J.C., Becker, K., Brown, D., Brügmann, G., Chiba, H., Fouquet, Y., Gemmell, J.B., Guerin, G., Hannington, M.C., Holm, N.G., Honnorez, J.J., Iturrino, G.J., Knott, R., Ludwig, R., Nakamura, K., Petersen, S., Reysenbach, A.-L., Rona, P.A., Smith, S., Sturz, A.A., Tivey, M.K., Zhao, X., 1995. The internal structure of an active sea-floor massive sulphide deposit. Nature 377, 713–716.

Jorge, R.C.G.S., Relvas, J.M.R.S., Barriga, F.J.A.S., 2005. Silica gel microtextures in siliceous exhalites at the Soloviejo manganese deposit, Spain. In: Mao, J., Bierlein, F.P. (Eds.), Mineral Deposit Research: Meeting the Global Challenge, vol. 1. Springer-Verlag, pp. 631–634. Chapter 69.

Kirkpatrick, J.D., Shipton, Z.K., Persano, C., 2009. Pseudotachylytes: rarely generated, rarely preserved or rarely reported? Bull. Seismol. Soc. Am. 99, 382–388. http://dx.doi.org/10.1785/0120080114.

Kirkpatrick, J.D., Rowe, C.D., White, J.C., Brodsky, E.E., 2013. Silica gel formation during fault slip: evidence from the rock record. Geology 41, 1015–1018.

Kirkpatrick, J.D., Rowe, C.D., 2013. Disappearing ink: how pseudotachylytes are lost from the rock record. J. Struct. Geol. 52, 183–198.

Korn, H., Martin, H., 1959. Gravity tectonics in the naukluft mountains of south West Africa. Bull. Geol. Soc. Am. 70, 1047–1078.

Manning, C.E., 1994. The solubility of quartz in H_2O in the lower crust and upper mantle. Geochimica Cosmochimica Acta 58, 4831–4839.

Martin, H., Porada, H., Wittig, R., 1983. Where lies the root zone of the Naukluft Nappe Complex. Spec. Publ. Geol. Soc. S. Afr. 11, 199–207.

Martin, H., Porada, H., 1977. The intracratonic branch of the Damara Orogen in South West Africa: I. Discussion of geodynamic models. Precambrian Res. 5, 311–338.

Micklethwaite, S., 2008. Optimally oriented "fault-valve" thrusts: evidence for aftershock-related fluid pressure pulses? Geochem. Geophys. Geosys. 9 (4), 10.

Miller, R.M., 1983. The Pan-African damara orogen of south West Africa/Namibia. Special publication. Geol. Soc. S. Afr. 11, 431–515.

Moore, J.C., Vrolijk, P., 1992. Fluids in accretionary prisms. Rev. Geophys. 30 (2), 113–135.

Mroczek, E.K., White, S.P., Graham, D.J., 2000. Deposition of amorphous silica in porous packed beds – predicting the lifetime of reinjection aquifers. Geochemistry 29, 737–757.

Niemeijer, A., Di Toro, G., Griffith, W.A., Bistacchi, A., Smith, S.A., Nielsen, S., 2012. Inferring earhtquake physics and chemistry using integrated field and laboratory approach. J. Struct. Geol. 39, 2–36. http://dx.doi.org/10.1029/j.jsg.2012.02.018.

Oehler, J.H., 1975. Origin and distribution of silica lepispheres in porcelanite from the monterey formation of California. J. Sediment. Petrol. 45 (1), 252–257.

Oehler, J.H., 1976. Hydrothermal crystallization of silica gel. Geol. Soc. Am. Bull. 87, 1143–1152. http://dx.doi.org/10.1130/0016-7606.

Otsuki, K., Monzawa, N., Nagase, T., 2003. Fluidization and melting of fault gouge during seismic slip: Identification in the Nojima fault zone and implications for focal earthquake mechanisms. J. Geophys. Res. 108 (B42192), 18. http://dx.doi.org/10.1029/2001JB001711.

Pec, M., Stünitz, H., Heilbronner, R., Drury, M., de Capitani, C., 2012. Origin of pseudotachylites in slow creep experiments. Earth Planet. Sci. Lett. 355–356, 299–310.

Poetsch, T., 2004. Forms and dynamics of silica gel in tuff-dominated soil complex: results of micromorphological studies in the Central Highlands of Mexico. Rev. Mex. Ciencias Geol. 21 (1), 195–201.

Potapov, V.V., 2004. Formation of solid deposits of amorphous silica in a flow of hydrothermal solution. Glass Phys. Chem. 30 (1), 82–89.

Power, W.L., Tullis, T.E., 1989. The relatiohsip between slickenside surfaces in fine-grained quartz and the seismic cycle. J. Struct. Geol. 11 (7), 879–893.

Rimstidt, J.D., Barnes, H.L., 1980. The kinetics of silica-water reactions. Geochimica Cosmochimica Acta 44, 1683–1699.

Ronacher, E., Richards, J.P., Johnston, M.D., 2000. Evidence for fluid phase separation in high-grade ore zones at the Porgera gold deposit, Papua New Guinea. Miner. Deposita 35, 638–688.

Rowe, C.D., Fagereng, Å., Miller, J.A., Mapani, B.S., 2012. Signature of coseismic decarbonation in dolomite fault rocks of the Naukluft Thrust, Namibia. Earth Planet. Sci. Lett. 333-334, 200–210.

Sahagian, D.L., Proussevitch, A.A., 1998. 3D particle size distributions form 2D observations: stereology for natural applications. J. Volcanol. Geotherm. Res. 84, 173–196.

Sander, M.V., Black, J.E., 1988. Crystallization and recrystallization of growth-zoned vein quartz crystals from epithermal systems – implications for fluid inclusion studies. Econ. Geol. 83 (5), 1052–1060.

Sherlock, R.L., Lehrman, N.J., 1995. Occurrences of dendritic gold at the McLaughlin Mine hot-spring gold deposit. Miner. Deposita 30, 323–327.

Sibson, R.H., Toy, V.G., 2006. The habitat of fault-generated pseudotachylyte: presence vs. absence of friction-melt. In: Abercrombie, R., McGarr, A., Kanamori, H., Di Toro, G. (Eds.), Earthquakes: Radiated Energy and the Physics of Faulting: Geophysical Monograph, vol. 170. American Geophysical Union, pp. 153–166.

Smith, S.A.F., Billi, A., Di Toro, G., Spiess, R., 2011. Principal slip zones in limestone: microstructural characterization and implications for the seismic cycle (Tre Monti fault, central Appenines, Italy). Pure Appl. Geophys. 168 (12), 2365–2393. http://dx.doi.org/10.1007/s00024-011-0267-5.

Stanistreet, I.G., Kukla, P.A., Henry, G., 1991. Sedimentary basinal responses to a late precambrian wilson cycle: the Damara orogen and Nama foreland, Namibia. J. Afr. Earth Sci. 13 (1), 141–156.

Stel, H., Lankreyer, A.C., 1994. Flow and deformation of viscous, silica-oversaturated dispersions in low-grade faults. J. Struct. Geol. 16 (3), 303–313.

Tryon, M.D., Brown, K.M., Torres, M.E., 2002. Fluid and chemical flux in and out of sediments hosting methane hydrate deposits on hydrate ridge, OR, II: hydrological processes. Earth Planet. Sci. Lett. 201, 541–557.

Ujiie, K., Yamaguchi, A., Kimura, G., Toh, S., 2007. Fluidization of granular material in a subduction thrust at seismogenic depths. Earth Planet. Sci. Lett. 259, 307–318.

Ujiie, K., Tanaka, H., Saito, T., subasa, Tsutsumi, A., Mori, J.J., Kameda, J., Brodsky, E.E., Chester, F.M., Eguchi, N., Toczko, S., Expedition 343 and 343T Scientists, 2013. Low coseismic shear stress on the Tohoku-Oki megathrust determined from laboratory experiments. Science 342 (6163), 1211–1214.

Viola, G., Mancktelow, N.S., Miller, J.A., 2006. Cyclic frictional-viscous slip oscillations along the base of an advancing nappe complex: insights into brittle-ductile nappe emplacement mechanisms from the Naukluft Nappe Complex, central Namibia. Tectonics 25. http://dx.doi.org/10.1029/2005TC001939.

Weatherley, D.K., Henley, R.W., 2013. Flash vaporization during earthquakes evidenced by gold deposits. Nat. Geosci. 6, 294–298.

Weibel, R., Friis, H., Kazerouni, A.M., Svendsen, J.B., Stokkendal, J., Poulsen, M.L.K., 2010. Development of early diagenetic silica and quartz morphologies – examples from the Siri Canyon, Danish North Sea. Sediment. Geol. 228, 151–170.

White, D.E., Brannock, W.W., Murata, K.J., 1956. Silica in hot-spring waters. Geochimica Cosmochimica Acta 10, 27–59.

White, L.A., Crerar, D.A., 1985. Silica diagenesis, II: general mechanisms. J. Sedimentol. 55 (3), 312–321.